JACS Au
AN OPEN ACCESS JOURNAL OF THE AMERICAN CHEMICAL SOCIETY

pubs.acs.org/jacsau
Article

Engineering of a Fluorescent Protein for a Sensing of an Intrinsically Disordered Protein through Transition in the Chromophore State

Tae-Geun Yu, Jinsu Lee, Jungmin Yoon, Jung Min Choi, Dong-Gun Kim, Won Do Heo, Ji-Joon Song, and Hak-Sung Kim*

Cite This: JACS Au 2023, 3, 3055−3065
Read Online

ACCESS | Metrics & More | Article Recommendations | Supporting Information

ABSTRACT: Intrinsically disordered proteins (IDPs) not only play important roles in biological processes but are also linked with the pathogenesis of various human diseases. Specific and reliable sensing of IDPs is crucial for exploring their roles but remains elusive due to structural plasticity. Here, we present the development of a new type of fluorescent protein for the ratiometric sensing and tracking of an IDP. A β-strand of green fluorescent protein (GFP) was truncated, and the resulting GFP was further engineered to undergo the transition in the absorption maximum upon binding of a target motif within amyloid-β (Aβ) as a model IDP through rational design and directed evolution. Spectroscopic and structural analyses of the engineered truncated GFP demonstrated that a shift in the absorption maximum is driven by the change in the chromophore state from an anionic (460 nm) state into a neutral (390 nm) state as the Aβ binds, allowing a ratiometric detection of Aβ. The utility of the developed GFP was shown by the efficient and specific detection of an Aβ and the tracking of its conformational change and localization in astrocytes.

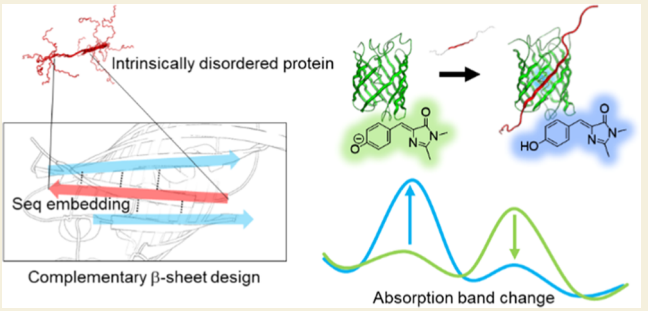

KEYWORDS: *protein design, protein engineering, fluorescent protein, intrinsically disordered protein, chromophore state, sensor protein*

1. INTRODUCTION

Intrinsically disordered proteins (IDPs) exist in incompletely folded states with undefined secondary structures, accounting for more than 44% of human proteome.[1] IDPs form dynamic complexes through interaction-induced local folding (folding-upon-binding) and play critical roles in a variety of biological processes.[2−5] However, their dysfunctional behaviors are linked with the pathogenesis of various diseases.[6] As typical IDPs, amyloid-β (Aβ) and α-synuclein undergo conformational changes into aggregates comprising stacked β-sheets, called amyloids. Such amyloidogenic proteins have been recognized as the hallmark of neurodegenerative diseases, including Alzheimer's and Parkinson's diseases.[7,8]

For a comprehensive understanding of the biological functions and pathological relevance of IDPs, specific and reliable sensing of IDPs are prerequisite. However, currently available approaches to sensing protein molecules have been developed mainly based on well-defined structural information typically found in globular proteins, and consequently, they are not applicable to the study of IDPs.[9−12] Unlike globular proteins, IDPs exist in a diverse range of conformational ensembles, displaying structural plasticity, promiscuous binding, and propensity to aggregate.[13,14] Such unusual characteristics have imposed difficulties in developing efficient methods for detecting and tracking of IDPs.[13,15,16] To date, most commonly used approaches include the attachment of fluorescent dyes or the genetic fusion of fluorescent proteins to IDPs, mainly focusing on visualization of their localization.[17−21] Nevertheless, these methods pose some drawbacks such as the need for complicated conjugation procedures and severe disruption of native IDP structures. Consequently, there is a strong quest for the simple and specific sensing of endogenous IDPs.

Here, we report a new type of fluorescent protein that allows specific and simple tracking of an IDP. As a template, green fluorescent protein (GFP) was employed, considering that its fragmented parts or a β-strand-truncated variant can form a complete β-barrel structure when complemented.[22,23] We hypothesized that this complementation process is similar to the binding mode of IDPs in that both the fragmented parts and truncated form of GFP exist in disordered states as IDPs and undergo the folding-upon binding to an interacting partner. Based on this, we truncated a β-strand of green

Received: August 5, 2023
Revised: September 18, 2023
Accepted: October 2, 2023
Published: October 26, 2023

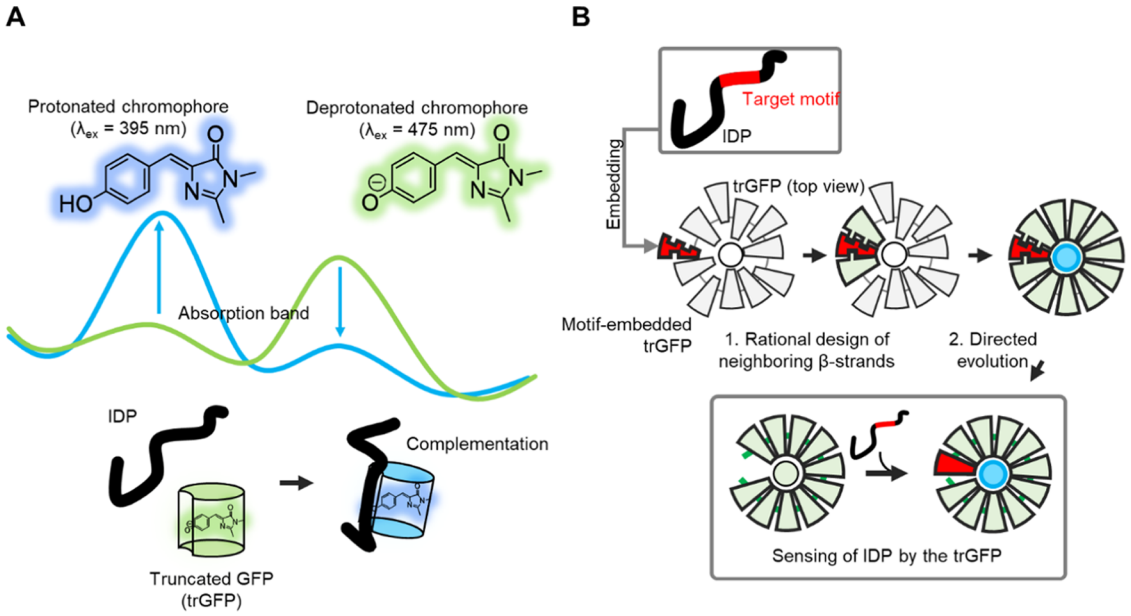

Figure 1. Schematic illustration of the development of a truncated GFP (trGFP) for the ratiometric sensing of Aβ. (A) A trGFP undergoes a shift in two absorption bands through the transition of the chromophore from a protonated (neutral) to a deprotonated (anionic) state upon complementation with a target motif within an IDP. (B) Two-step strategy involving a rational design and directed evolution for developing a trGFP for the ratiometric sensing of Aβ.

fluorescent protein (GFP) and further engineered the resulting truncated GFP through a rational design and directed evolution to undergo the change in the absorption maximum upon binding of a target motif in Aβ as a model IDP. The spectroscopic and structural analyses of the engineered GFP demonstrated that a shift in its absorption maximum is driven by the transition in the chromophore state from an anionic into a neutral one as the Aβ binds. We showed the utility of the developed GFP by detecting and tracking the conformational change and localization of Aβ in astrocyte cells in a highly specific and distinct manner, which has been difficult by existing methods. Details are reported herein.

2. RESULT

2.1. Strategy for the Design of a Truncated GFP for the Ratiometric Sensing of Aβ

As a proof of concept, we aimed to develop a truncated form of GFP that undergoes a shift in the absorption bands when complemented with a target motif within Aβ, enabling the ratiometric sensing of Aβ (Figure 1A). Aβ is produced by the proteolytic digestion of a transmembrane protein (amyloid precursor protein) and then released into extracellular space. Although Aβ is one of the best-known IDPs, its sensing and analysis have been a challenge due to its tiny size and structural plasticity.[6,24] Due to the unstable structural characteristics of IDPs, rapid signal response is essential for their accurate detection. Typical β-strand-truncated GFPs are known to undergo chromophore maturation after the complementation, requiring a lengthy duration of time.[23,25] In contrast, β-strand-truncated GFPs with matured chromophore frequently exhibit a high background fluorescence, resulting in low signal-to-noise ratios, even in the absence of a complementing peptide.[26,27] Such truncated GFPs are known to retain partial structure and prone to significant photoexcitation via anionic chromophores.[28−30]

To address these issues, we intended to develop ratiometric fluorescence sensing of Aβ instead of a traditional single-wavelength fluorescence measurement. A ratiometric sensing provides a self-calibrating feature, significantly reducing the background noise and artifacts.[31,32] The absorption spectrum of the GFP's chromophore is determined by the protonation state of its phenol group, displaying the protonated A state (neutral) and deprotonated B state (anionic) with absorption maxima at around 395 and 475 nm, respectively.[33] The protonation state of the chromophore (chromophore's pK_a value) is influenced by the arrangement of the surrounding amino acids. We thus hypothesized that a truncated form of GFP which favors a neutral chromophore when complemented with a target motif would result in an increase in the ratio of a neutral to an anionic state of the chromophore in response to the increasing Aβ level compared to the uncomplemented state.

Our design strategy involves two steps (Figure 1B): First, a target motif sequence of an Aβ is embedded into a β-strand-truncated GFP to generate a motif-embed-truncated GFP and the neighboring β-strands of the truncated GFP are optimized to accommodate the motif. Next, the resulting truncated GFP is subjected to a directed evolution for the selection of a truncated GFP showing the highest change in the absorbance band in the presence of the embedded motif.

2.2. Rational Design and Directed Evolution of a trGFP Accommodating an Aβ Motif

We first constructed a truncated form of GFP by deleting seventh β-strand from circularly permutated GFP derived from superfolder GFP (sfGFP) as previously described.[34] We reasoned that such a truncated GFP (trGFP) would be suited for our goal based on the observation that the seventh β-strand has a crucial position for modulating the protonation state of the chromophore (H148, numbered according to sfGFP).[35] In addition, the chromophore of a seventh β-strand deleted GFP was known to mature spontaneously during expression.[36] To

https://doi.org/10.1021/jacsau.3c00445
JACS Au 2023, 3, 3055−3065

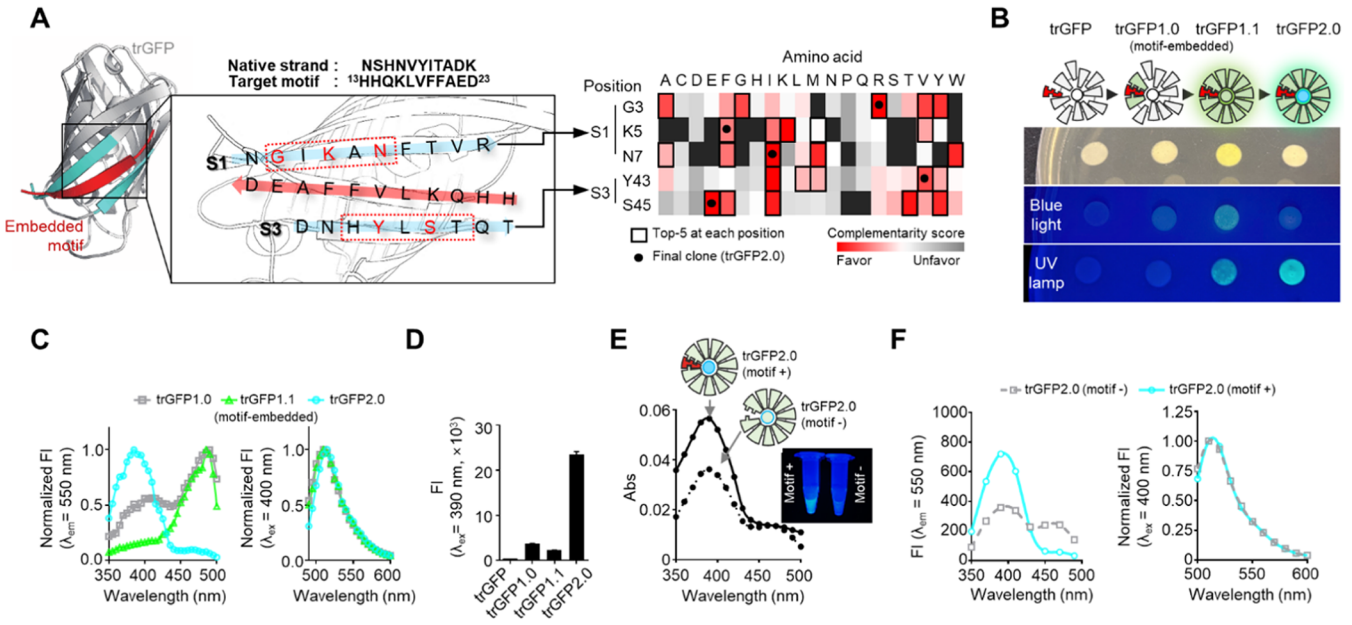

Figure 2. Development of a trGFP for ratiometric sensing of Aβ through a two-step procedure involving rational design and directed evolution. (A) Design of a trGFP accommodating an Aβ motif through a rational design of neighboring β-strands using the B-SIDER algorithm. The model structure of the motif-embedded trGFP is presented on the left. The embedded target motif sequence (red) is surrounded by the 1st (S1) and 3rd (S3) β-strands of the trGFP. The β-sheet complementarity scores for mutations at five positions (G3, K5, N7, Y43, and S45, shown in red) were calculated using the B-SIDER algorithm and are presented as a heat map (right). Selected amino acid residues at five positions in the final clone (trGFP2.0) are marked. Black colors indicate a penalty score. (B) *E. coli* cells expressing the selected clones (motif-embedded trGFPs) during rational design and directed evolution. (C) Excitation and emission spectra of the selected clones (FI, fluorescence intensity; left, excitation; right, emission). (D) Fluorescence emission of selected clones when excited at 390 nm. The data represent mean ± SD (n = 3). (E) Absorption spectra of the trGFP2.0 and motif-embedded trGFP2.0 (0.6 μM in DPBS), respectively. The inset image was taken under a UV lamp. (F) Emission (left) and excitation (right) spectra of the trGFP2.0 and motif-embedded trGFP2.0 (200 nM in DPBS), respectively. Data points indicate the means in triplicate measurements, and standard errors were omitted for clarity (E, F).

determine a specific sequence motif in an Aβ to be embedded into the trGFP, a series of 11-residue sequence motifs were examined by a moving window along the Aβ sequence in terms of the complementarity to nearby β-strands of the trGFP using the B-SIDER algorithm (Figure S1).[37,38] As a result, ^{13}HHQKLVFFAED^{23} motif within Aβ was finally selected as a target motif to be embedded into the trGFP (Figure 2A and Table S1). The target motif was embedded through genetic fusion by replacing the native seventh β-strand downstream of the sixth β-strand. The motif-embedded trGFP was observed to emit negligible fluorescence when expressed in *Escherichia coli*, implying that the embedded motif sequence does not fit well. We thus used the B-SIDER algorithm to rationally optimize the two neighboring β-strands of the trGFP to maximize the complementarity to the motif sequence. In our previous study, the B-SIDER algorithm, which is a sequence-based complementary β-sheet design approach, was shown to be effective for a redesign of the β-strands of GFP.[37] In addition, owing to the presence of the chromophore in this case, a sequence-based approach focusing on the neighboring β-strands could result in a favorable outcome, whereas a structure-based optimization would be tricky. In order to avoid any perturbations in core side-chain packing, outward amino acids on the neighboring β-strands (G3, K5, N7, Y43, and S45) were chosen for optimization. The motif-embedded trGFP was modeled, and the β-sheet complementarity resulting from mutations at the selected mutation sites was evaluated using the B-SIDER algorithm (Figure S2). Based on the B-SIDER scoring matrix, we predicted the amino acids to be substituted at the mutation sites for a higher β-sheet complementarity (Figure 2A, right). A focused mutant library was constructed using degenerate codons containing the top-5 amino acids in terms of score at each position. The library was transformed into *E. coli*, followed by plating on selective media containing IPTG. Under blue light at approximately 450 nm, we visually selected an initial clone, designated as trGFP1.0 (Table S2). The motif-embedded trGFP1.0 emitted a marginal fluorescence under blue light and folded stably into a monomer (Figures 2B and S3).

To improve the stability and fluorescence intensity of trGFP1.0, we conducted four rounds of directed evolution using error-prone PCR (epPCR) and selected a clone emitting a significantly increased fluorescence in the presence of embedded motif, which was designated as trGFP1.1 (Figure 2B and Table S2). However, motif-embedded trGFP1.1 was observed to still favor an anionic chromophore state with a biased excitation at about 480 nm (Figure 2C). Therefore, directed evolution was further performed for trGFP1.1 to alter the preference of its chromophore state toward a neutral state when it was complemented with the Aβ motif (Table S3). The target motif was embedded through genetic fusion, as described earlier. However, in this instance, a flexible linker with an extended length was fused to the N-terminus of trGFP1.1 to efficiently screen positive clones (Table S1). We screened the clones using a UV light with a wavelength of approximately 365 nm and finally selected a clone, termed trGFP2.0. The motif-embedded trGFP2.0 exhibited a significantly enhanced absorbance at 390 nm (Figure 2B–D), and spectroscopic analysis confirmed that it shows a biased excitation at the A band (protonated, neutral chromophore)

https://doi.org/10.1021/jacsau.3c00445
JACS Au 2023, 3, 3055−3065

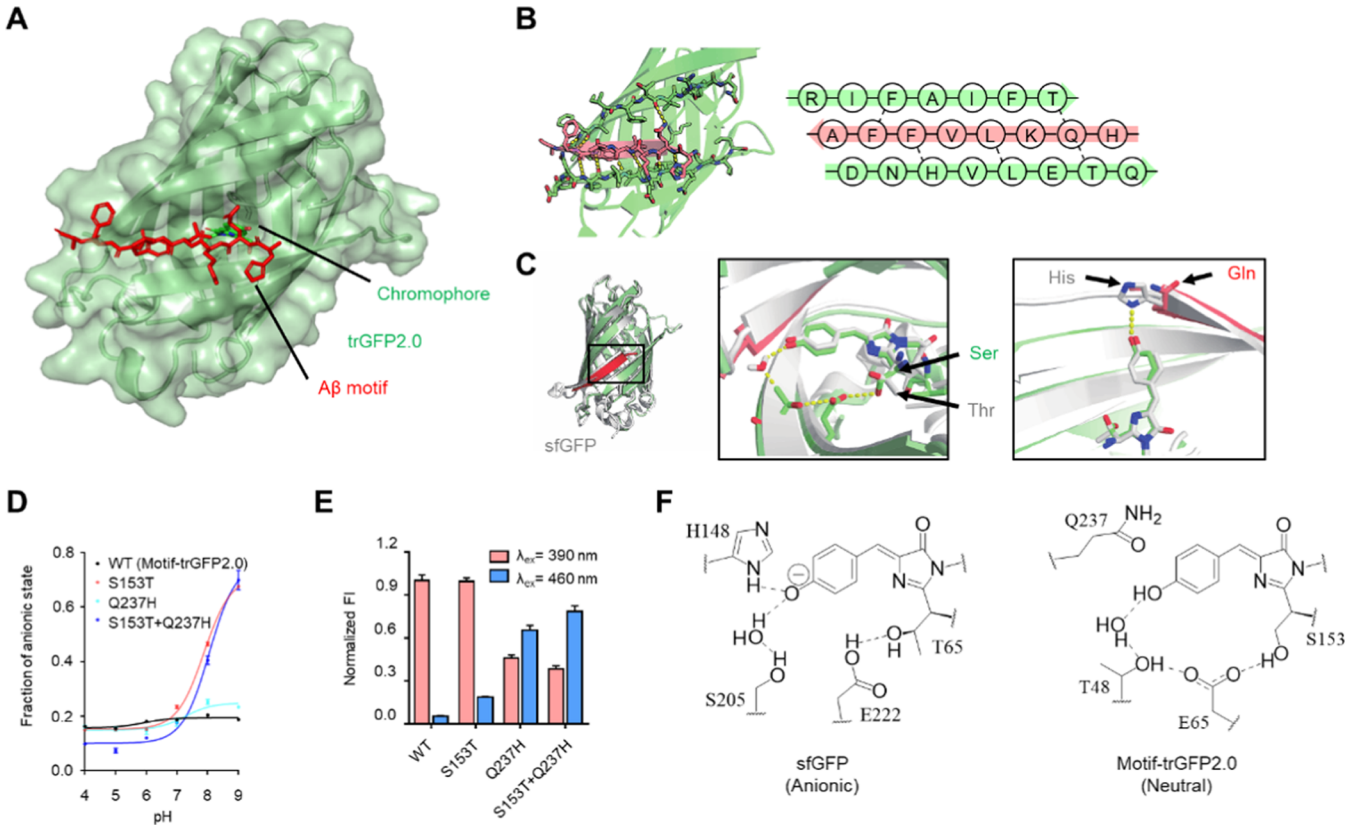

Figure 3. Structural basis of the underlying mechanism for the transition in a chromophore state of the trGFP2.0. (A) Cartoon representation of the crystal structure of the trGFP2.0 in complex with the Aβ motif. (B) Interaction between the Aβ motif and adjacent β-strands. The Aβ motif is highlighted in a red arrow. (C) Structural alignment of sfGFP (PDB ID: 2B3P, gray) with the trGFP2.0 in complex with the Aβ motif. The major amino acid changes near the chromophore are shown in the insets. The hydrogen-bonding network is depicted using dashed yellow lines. (D) Relative fraction of an anionic chromophore state ($Abs_{480}/(Abs_{390}+Abs_{480})$) in motif-embedded trGFP2.0 variants with respect to pH. (E) Fluorescence emission from the motif-embedded trGFP2.0 variants when excited at 390 and 460 nm, respectively. (F) Structural formulas depicting the chromophores of the motif-embedded trGFP2.0 and sfGFP along with their respective surrounding residues. The data represent the mean ± SD in triplicate experiments (D, E).

(Figure 2C). Among a total of nine mutations in the trGFP2.0, five were found to originate from the first optimization process using B-SIDER, and the rest resulted from the directed evolution procedure (Figure S4 and Table S2).

2.3. Spectroscopic Features of the trGFP2.0

We investigated the spectroscopic characteristics of the trGFP2.0. As expected, the trGFP2.0 was observed to display a distinct absorption peak at 390 nm, but its absorbance was much lower than the motif-embedded trGFP2.0 (Figure 2E). The motif-embedded trGFP2.0 showed a strong absorbance preference at the A band (390 nm), whereas the trGFP2.0 displayed a significantly decreased absorbance ratio between the A and B bands, implying a change in pK_a of the phenol group in the chromophore. We thus investigated the effect of pH on the absorption spectra of both the trGFP2.0 and motif-embedded trGFP2.0 and observed that the pK_a value of the chromophore decreased in the absence of the Aβ motif, modulating the protonation state of the chromophore (Figure S5). Variations in the ratios of the absorbance spectra were shown to result in a large difference in the fluorescence excitation spectra, whereas the change in the emission spectra was negligible (Figure 2F). The extinction coefficients and quantum yields of trGFP2.0 were measured (Table S4). Based on the results, it is likely that the trGFP2.0 underwent a significant transition in the chromophore state, consequently leading to a shift in an excitation spectrum when complemented with the Aβ motif, which implies its utility as a ratiometric fluorescence sensor for an Aβ.

2.4. Crystal Structure of the trGFP2.0 in Complex with Aβ Motif

To obtain insight into the mechanism through which the spectroscopic feature is driven, we determined the crystal structure of trGFP2.0 in complex with an Aβ motif. To mitigate the self-oligomerization of the Aβ motif and promote the stable formation of the binding complex, we genetically fused the target motif to the N-terminus of trGFP2.0 using a flexible linker (Table S1). Following purification, the linker was removed as previously described elsewhere.[30] The trGFP2.0 was shown to form a 1:1 complex with the target motif (Figure S6). The crystal structure indicates that the target motif is bound to a vacant space of trGFP2.0, forming a complete β-barrel structure, which shows the complementation of trGFP2.0 with the target Aβ motif (Figure 3A). The residue pairing of β-strands surrounding the target motif was observed to be formed as intended (Figure 3B). To demonstrate an increase in pK_a of the chromophore when the trGFP2.0 is complemented with the target motif, the structure of the trGFP2.0 in complex with a target motif was compared with sfGFP (PDB ID: 2B3P),[39] which is a parental GFP variant of the trGFP2.0 and shows a strong preference for the anionic

https://doi.org/10.1021/jacsau.3c00445
JACS Au 2023, 3, 3055−3065

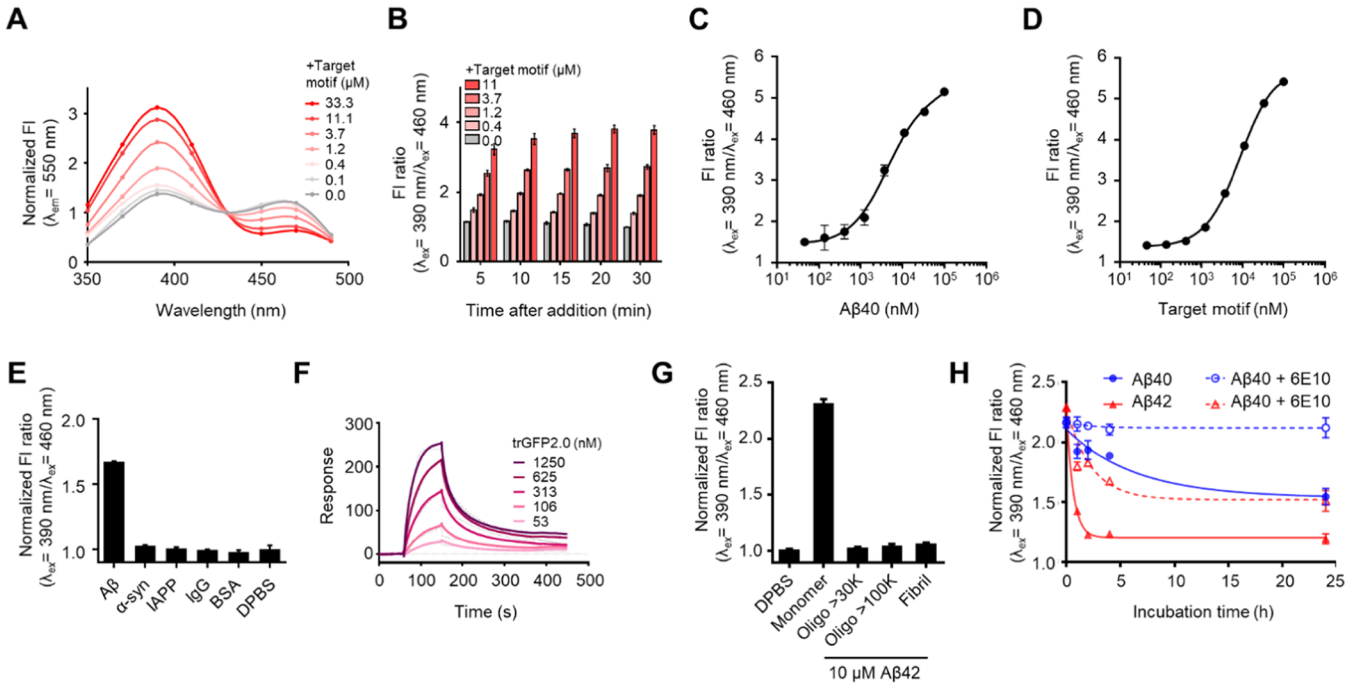

Figure 4. Ratiometric sensing of Aβ using the trGFP2.0. (A) Changes in the excitation spectra of the trGFP2.0 in the presence of different concentrations of the Aβ motif. The relative fluorescence intensity (FI) was measured 20 min after the addition of Aβ motif and normalized by the value at 430 nm. Data points represent the means in triplicate measurements. Standard errors were omitted for clarity. (B) Change in the FI ratio by the trGFP2.0 in the presence of different concentrations of the Aβ motif at varying incubation times. (C) Change in the FI ratio by the trGFP2.0 in the presence of different concentrations of the Aβ40 and target motif (D). (E) Normalized FI ratio by the trGFP2.0 in the presence of 8 μg/mL of Aβ40, α-synuclein (α-Syn), Islet Amyloid Polypeptide (IAPP), human immunoglobulin G (IgG), bovine serum albumin (BSA), or equal volume of DPBS. (F) Representative SPR sensogram of the trGFP2.0 for the Aβ motif. (G) Normalized FI ratio by the trGFP2.0 in the presence of fibrils, oligomers, and monomers of Aβ42. (H) Monitoring a conformational change of the Aβ42 through the trGFP2.0. 20 μM Aβ42 was incubated at 37 °C and 200 rpm. The solution was then sampled at the designated time. The sampled solutions were mixed with trGFP2.0, and normalized FI ratio was measured. "6E10" indicates anti-Aβ antibody. The data represent the mean ± SD in triplicate experiment (B, E, G, and H) and quadruplicate (C, D).

chromophore state. While the two structures are found to share almost an identical fold (Figure 3C, RMSD = 1.564 Å), the major differences are the first amino acid residue of the chromophore and a substitution of histidine for glutamine, which is located in the seventh strand of the sfGFP (counterpart is the complexed target motif in the trGFP2.0 structure) (Figure 3C, inset). These two substitutions seem to directly alter the microenvironment around the chromophore. To test whether the difference in the corresponding amino acids is responsible for an increase in pK_a of the motif-embedded trGFP2.0 chromophore, namely, the preference for a neutral chromophore, we introduced back mutations (S153T and Q237H) into the motif-embedded trGFP2.0. The resulting variants were expressed and purified, and the change in the protonation state of the respective chromophores was analyzed with respect to pH (Figure 3D). At the same time, the fluorescence emissions from the variants were measured when excited at 390 and 460 nm to check whether the change in fluorescence excitation was caused by the protonation state of the chromophore (Figure 3E). As a result, the variants showed a decreased preference for a neutral chromophore, and S153T gave rise to a greater change, which are in line with previous reports.[40,41] The presence of threonine in the chromophore was reported to significantly decrease the pK_a of the chromophore and prevent the neighboring glutamate from acting as a proton acceptor in the excited-state proton transfer (ESPT).[40] It thus is likely that the serine residue next to the chromophore of motif-embedded trGFP2.0 served as a gatekeeper for the effective ESPT and the preference for a neutral chromophore. On the other hand, histidine of seventh strand, which assists in stabilizing an anionic chromophore state,[41] disappeared in the aforementioned substitution of glutamine for histidine. As proposed in Figure 3F, the trGFP2.0 was shown to undergo a strong photoexcitation in the neutral chromophore state when complemented with the target motif, and this seems to be due to an efficient ESPT potentially resulting from serine residue next to the chromophore and destabilization of the anionic chromophore state through histidine substitution.

2.5. Ratiometric Fluorescence Sensing of Aβ through the trGFP2.0

We tested whether trGFP2.0 can be used for the ratiometric fluorescence sensing of Aβ in a solution. For this, the target Aβ motif was genetically fused to a highly soluble protein called a "repebody" to prevent self-oligomerization, and the resulting construct was expressed in *E. coli* and purified as described elsewhere.[42] The trGFP2.0 was mixed with increasing concentrations of the repebody-fused target motif, and the fluorescence emission was measured when excited at different wavelengths (Figure 4A). Fluorescence intensities of trGFP2.0 were shown to change in the opposite direction with the increasing motif concentration when excited at the A and B bands, respectively. Based on these spectroscopic features, we determined the ratio of the fluorescence emission intensity at different times as the ratiometric fluorescence signal for the Aβ

https://doi.org/10.1021/jacsau.3c00445
JACS Au 2023, 3, 3055−3065

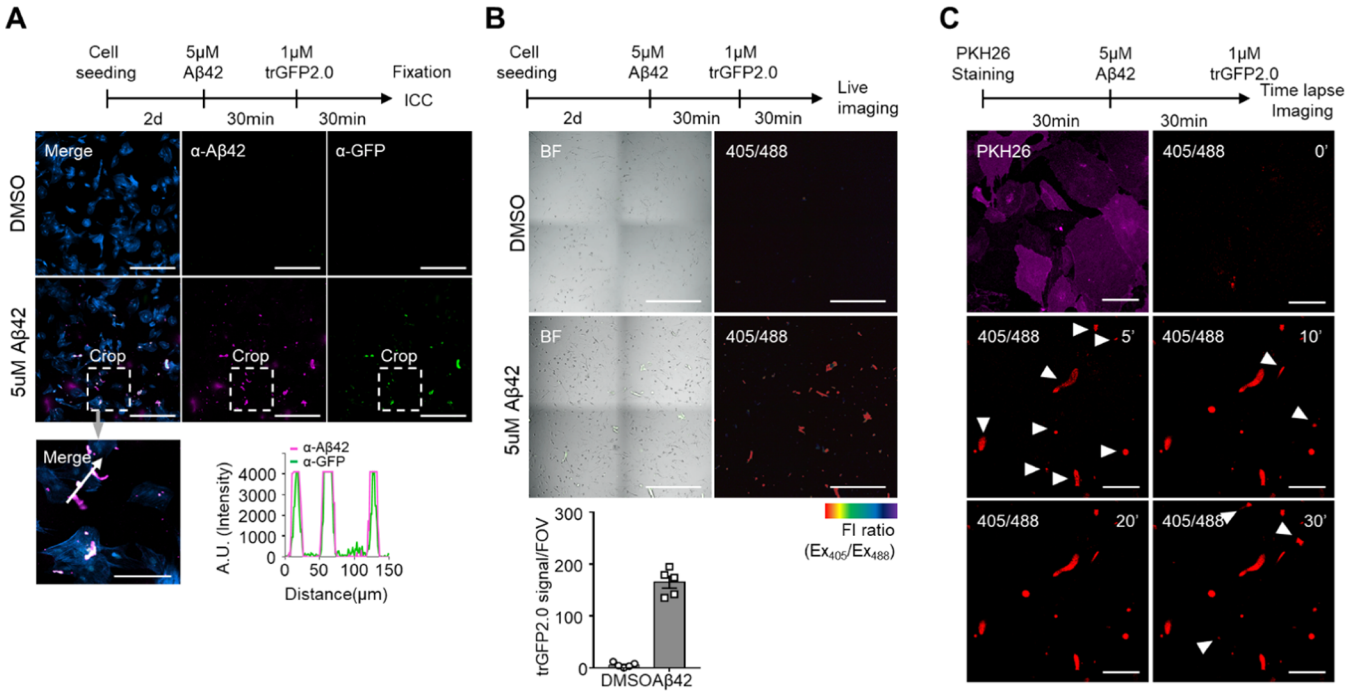

Figure 5. Tracking the spatial localization of a label-free Aβ by the trGFP2.0. (A) Immunocytochemistry of mouse astrocytes treated with the trGFP2.0 after the addition of Aβ42 to an extracellular space. Anti-βIII-Tubulin, anti-Aβ, and an anti-GFP antibody were used for staining the cytosol (blue in the merged image), Aβ42 (purple), and trGFP2.0 (green), respectively. A cross-sectional analysis was conducted to assess the colocalization of Aβ42 with the trGFP2.0 (right bottom). (B) Live cell imaging of mouse astrocyte treated with the trGFP2.0 after the addition of Aβ42. The fluorescence intensity (FI) ratio (405/488) by the trGFP2.0 was obtained through excitation at 405 and 488 nm, respectively. "BF" indicates a bright field view image. The trGFP2.0 signal/field of view (FOV) was counted through object count function. The data represent the mean ± SEM from random eight FOV. (C) Time-lapse live cell imaging of mouse astrocytes treated with the trGFP2.0 after the addition of Aβ42. The time points in minutes are shown in the top right of each image. PKH26 was used for staining of the cell membrane. The white arrowhead indicates the newly emerged trGFP2.0 signal. Scale bars indicate 200 μm (A, C) and 500 μm (B), respectively.

motif after the addition of the trGFP2.0 when excited at 390 and 460 nm, respectively (Figure 4B). The fluorescence intensity ratio was shown to increase in proportion to the concentration of the Aβ motif and reached the maximum after 20 min. In the following experiments, the fluorescence intensity ratio was measured 20 min after the addition of trGFP2.0 to obtain reliable signals. For comparison with the intensiometric fluorescence measurement, we assessed the change in fluorescence intensity when excited at a single wavelength (Figure S7). As expected, the fluorescence intensity excited at a single wavelength showed only a slight change due to the presence of a high background fluorescence. The trGFP2.0 was observed to have stably maintained the spectroscopic performance in various buffers and even after 7 days of storage at room temperature (Figures S8−S10).

We next examined if the trGFP2.0 can also recognize Aβ40 comprising 40 amino acid residues, which is a predominant Aβ form. The trGFP2.0 was mixed with different concentrations of Aβ40 or Aβ motif, and the ratio of fluorescence intensity was measured (Figure 4C,D). The fluorescence intensity ratio increased in a sigmoidal manner with the increasing concentration of Aβ40, displaying a pattern similar to that of the Aβ motif. These results indicate that trGFP2.0 recognizes both Aβ40 and the Aβ motif, showing a distinct change in the fluorescence intensity ratio. We tested the specificity of the trGFP2.0 for various amyloidogenic proteins (Figures 4E andS11). The trGFP2.0 exhibited specificity for Aβ, while giving rise to negligible signals for other IDPs, amyloidogenic proteins, and an off-target motif within Aβ40, which validates our design strategy. We next checked the interaction between the trGFP2.0 and Aβ through surface plasmon resonance (SPR) (Figure 4F). The reassembly of split GFP with a paired peptide was revealed to result in irreversible binding.[22] As the primary objective of trGFP2.0 is to detect a specific peptide motif, we intended to avoid irreversible binding. Consequently, we assessed the interaction between trGFP2.0 and the target motif to validate the reversibility. The binding between trGFP2.0 and the Aβ motif showed a reversible association/dissociation. The association and disassociation rate constants were estimated to be 6.7×10^7 M^{-1} s^{-1} and 14.3 s^{-1}, respectively. We further confirmed that a specific interaction with trGFP2.0 could suppress Aβ fibrillation (Figure S12).

2.6. Monitoring the Conformational Change of Aβ Using the trGFP2.0

We next tested whether the trGFP2.0 can be used for monitoring the conformational change of a target IDP. Solvent accessibility to a specific motif in an IDP is known to vary with its structural state.[43] Hence, the inherent ability of trGFP2.0 to selectively interact with the target motif holds significant promise in the monitoring of structural alterations within IDP. The target Aβ motif used in this study is within the midregion of the Aβ, initiating the oligomerization forming repetitive β-sheet structure, and is rapidly buried inside as oligomerization of the Aβ occurs.[44] We thus reasoned that trGFP2.0 will be preferentially complemented with a fully stretched form of Aβ (i.e., monomeric form), featuring an exposed target motif. Further, the envisaged interaction was expected to facilitate the

https://doi.org/10.1021/jacsau.3c00445
JACS Au 2023, 3, 3055−3065

sensitive monitoring of the initiation of Aβ oligomerization by evaluating the accessibility of the target motif.

We first analyzed the fluorescence signals using trGFP2.0 against Aβ fibrils, oligomers, and monomers. For this, Aβ42 was incubated overnight at 37 °C with shaking (200 rpm), followed by sedimentation to obtain the fibrils and subsequent filtration using a molecular weight cutoff (MWCO) membrane to separate the oligomers of Aβ42. Freshly prepared Aβ42 monomers were used as a control. The trGFP2.0 emitted high fluorescence signals only for Aβ42 monomers (Figure 4G), whereas an extremely low signal change was observed even for small-sized oligomers separated through a 30 K MWCO filtration. To check the effect of the degree of Aβ42 oligomerization, the signal change was measured after the trGFP2.0 was mixed with a solution containing Aβ42 with different degrees of oligomerization (Figure S13A). To this end, Aβ42 was incubated at 37 °C while being shaken, and the solution was sampled at time intervals and added to the trGFP2.0. As a result, a lower fluorescence signal was observed for the samples that had been incubated for a longer time. A decrease in the fluorescence of the trGFP2.0 followed a typical monomer depletion pattern during amyloidogenesis, as previously reported.[45,46] Based on the results, we traced the monomer depletion pattern of Aβ under different conditions using the trGFP2.0. Two major isoforms of Aβ include Aβ40 and Aβ42, and Aβ42 is known to be more prone to aggregation than Aβ40. We tested both Aβ40 and Aβ42 to check if the trGFP2.0 can distinguish the differences in oligomerization kinetics (Figure 4H). The trGFP2.0 indeed showed a faster signal reduction for Aβ42 than for Aβ40, and the decrease in the slope was slowed by the addition of an anti-Aβ antibody (6E10), which is consistent with an earlier study.[47] In a similar manner, we could also efficiently monitor the enhanced progression of Aβ40 oligomerization in the presence of fibril seeds or metal ions (Figure S13B−E). The nucleation by metal ions (Cu^{2+} and Zn^{2+}) and the occurrence of secondary nucleation by the fibril seeds are recognized as a prominent factor influencing the kinetics of IDP oligomerization.[6] Particularly, in the case of the early stage transition by metal ions, it is difficult to observe by existing techniques, because metal ions are known to rapidly sequester Aβ monomers, leading to the formation of amorphous off-pathway oligomers instead of the characteristic β-sheet-rich structure of amyloid fibrils.[48−50] Nevertheless, the trGFP2.0 was proven to be highly effective in monitoring the conformational change of Aβ under various conditions. Based on the results, trGFP2.0 is likely to be used in monitoring the conformational change and structural transition of IDPs.

2.7. Tracking the Spatial Localization of a Label-free Aβ42 Using the trGFP2.0

We intended to track the spatial distribution of Aβ42 in cells using the trGFP2.0. When Aβ42 is added to an extracellular space, it is known to be rapidly localized on the cell membrane, particularly in ganglioside-rich lipid rafts.[51] This finding aligned with our own observation (Figure S14). The attachment of a monomeric Aβ to the cell membrane during the early stage is a crucial event for exploring the fate of the Aβ.[52] Nonetheless, conventional methods are difficult to monitor this event since they need a fusion of tag or multiple steps, such as fixation, which limits their applicability or accuracy.[17−20] To verify whether trGFP2.0 can trace the localization of Aβ42, we applied immunocytochemistry to cells that had been treated with trGFP2.0 after the addition of Aβ42 (Figure 5A). As a result, the trGFP2.0 was shown to colocalize with Aβ42, verifying the utility of the trGFP2.0 in tracking the spatial distribution of Aβ42. The amounts of Aβ42 tethered to the cell membrane and colocalized trGFP2.0 were observed to increase in a concentration-dependent manner with the increasing concentration of Aβ42 (Figure S15).

We next tested if the trGFP2.0 can act as a mix-and-measure-type sensor for label-free Aβ42 in live cell imaging. The trGFP2.0 undergoes a transition in the chromophore state upon the binding of Aβ42. We thus reasoned that trGFP2.0 could visualize the spatial distribution of extracellular Aβ through live cell imaging without additional fixation or labeling steps. We first checked if the changes in the fluorescence signal by trGFP2.0 could be analyzed by a confocal microscope using bead-immobilized trGFP2.0. As anticipated, the fluorescence emission ratio by the trGFP2.0 significantly varied upon interaction with the target motif, and this change was clearly observed through the confocal microscope (Figure S16). Following the addition of Aβ42 to the extracellular space of primary astrocytes, the trGFP2.0 was added, and the ratiometric fluorescence changes were monitored through excitation at 405 and 488 nm, respectively (Figures 5B and S17). The spatial location of Aβ42, which had been tethered to the cell surface, was clearly visualized by the trGFP2.0. It is noteworthy that images obtained with single-wavelength fluorescence, when excited either at 405 or 488 nm, had a much lower resolution (Figure S18). We also monitored the signal changes over time through time-lapse imaging (Figures 5C and S19). The trGFP2.0 was shown to quickly bind to Aβ42, displaying fluorescence signals within a few minutes, and the fluorescence intensity became stronger with time, supporting that the trGFP2.0 can be effectively used for tracking the spatial localization of a label-free Aβ42.

3. DISCUSSION

We showed the development of a new type of fluorescent protein for the simple and specific sensing of Aβ, a typical IDP, through a rational and directed evolution approach. Although the sensing and tracking of IDPs with high specificity are crucial for exploring their biological functions and pathological relevance, it has remained a challenge. The design of a trGFP that is complementary to a specific motif in IDP is a promising tactic for the development of a self-reported protein biosensor. Based on the spectroscopic feature of GFP in terms of the chromophore state, we successfully developed the trGFP2.0 which enables the sensing and tracking of Aβ in a ratiometric manner. The crystal structure of trGFP2.0 in complex with an Aβ motif demonstrated the mechanism by which the chromophore state undergoes transition from an anionic state to a neutral one when complemented with the Aβ motif. The trGFP2.0 indeed allowed the sensing of Aβ as well as the tracking of the oligomerization and localization of Aβ in astrocyte cells in a highly distinct manner, which have been difficult to achieve by existing methods. While the present study focused on the Aβ motif as a model, our approach seems to have the potential to extend to diverse IDPs. The present work provides insight into the design of a fluorescent protein for the specific detection and tracking of an IDP.

For the development of a fluorescent protein for the ratiometric sensing of Aβ, we considered several key factors. A matured chromophore is favorable for rapid fluorescence emission upon complementation with a target motif. Further, a

https://doi.org/10.1021/jacsau.3c00445
JACS Au 2023, 3, 3055−3065

ratiometric fluorescence measurement based on the change in the absorbance band in the presence of Aβ is crucial for the reliable and specific sensing of Aβ because of its self-calibrating ability compared to single-color fluorescence emission. Despite much effort, however, the rational design of such a trGFP has been difficult, mainly owing to the tricky β-sheet design and poor understanding of the microenvironment around the chromophore. In the present work, we first redesigned a β-strand-truncated GFP candidate through a rational sequence-based approach, followed by directed evolution. Complementation with an exogenous peptide was achieved using a complementary β-sheet design algorithm, and the trGFP2.0 showing the highest changes in a chromophore state upon binding of an Aβ was successfully obtained through directed evolution.

It is worthwhile to emphasize that our design strategy allowed for the development of a simple and effective self-reporting protein in contrast to conventional protein biosensors, which have complicated structures and multiple modules. The design principle of trGFP2.0 and the underlying molecular mechanism based on its crystal structure will provide insight into the development of fluorescent proteins for other target motifs in other IDPs. The trGFP2.0 can be simply integrated with other techniques, such as single-molecule fluorescence measurements and immunoassays, for analyzing various IDPs. With total internal reflection fluorescence (TIRF) microscopy, exceedingly low concentrations of Aβ in samples could be quantified by counting the number of trGFP2.0 molecules, showing the change in the fluorescence intensity at the single-molecule level. Taken together, our strategy can be extended to a variety of peptide motifs, including IDPs and unstructured regions of proteins, for exploring the biological functions and pathological relevance of IDPs.

4. EXPERIMENTAL SECTION

4.1. Gene Construction, Protein Expression, and Purification

IgG from human serum, IAPP, and BSA were purchased from Sigma-Aldrich, Abcam, and GenDEPOT, respectively. All constructs derived from trGFP were cloned into a pET28a vector, and a hexa-histidine tag was introduced at the N-terminus for affinity purification. Protein sequences used in this study are shown in Table S1. The α-synuclein construct was cloned into pET28a, as described above. The target amyloid motif and off-target motif were genetically fused to the C-terminus of a repebody with a linker containing Gly-Gly-Ser for soluble expression and purification. The constructs were then inserted into a pET21a vector, and a hexa-histidine tag was introduced at the C-terminus. The vector harboring the gene constructs was transformed into BL21 (DE3) cells, and the resulting cells were cultured in Luria−Bertani (LB) medium overnight. The culture medium was transferred to a fresh LB medium and cultured until the optical density at 600 nm reached 0.4−0.8. The cells were treated with 0.2 mM IPTG and further grown overnight at 18 °C. The cells were then harvested and disrupted through sonication in a buffer containing 50 mM Tris, 300 mM NaCl, and 5 mM imidazole. Cell-free extracts were obtained through the centrifugation of the cell lysate at 18,000g for 1 h followed by affinity purification. Ni-NTA agarose resin (Qiagen) was manually packed on a disposable column (Thermo Scientific), and bound proteins were washed with a buffer containing 50 mM Tris, 300 mM NaCl, and 10 mM imidazole. The resin-bound proteins were eluted with a buffer containing 50 mM Tris, 300 mM NaCl, and 150 mM imidazole, followed by purification through a size exclusion column (Superdex 200 Increase 10/300 GL column, Cytiva) with phosphate-buffered saline (DPBS). No unexpected or unusually high safety hazards were encountered.

4.2. Sequence Design of an Interacting β-Strand

Sequences of β-strands interacting with the embedded motif were designed using the same method as previously described with a slight modification.[37] The first and third β-strands of trGFP are in contact with the embedded motif, and amino acid residues on the two β-strands were primarily optimized to accommodate the embedded motif (Figures S1). Given that the embedded motif has partial interactions with two neighboring β-strands, we optimized the following interactions between β-strands: the first β-strand of trGFP ^{1}KNGIKANFT^{9} and the target motif KLVFFAEDV, the third β-strand of trGFP ^{40}DNHYLSTQT^{48}, and the target motif HHQKLVFFA. Then, five outward residues showing key interactions were selected for further optimization, i.e., Gly3, Lys5, Asn7, Tyr43, and Ser45. Because the second and fourth β-strands are in contact with the first and third β-strands of trGFP, respectively, we simultaneously considered the complementarity score between an amyloid motif and the first and second β-strands, as well as a target motif and the third and fourth β-strands. The complementarity scores of each site to be designed were calculated as the equally weighted sum of the B-SIDER scores from both in-contact β-strands.

4.3. Directed Evolution

A template trGFP1.1 gene was synthesized by IDT Technologies. A library of trGFP1.1 was constructed by overlap-PCR using primers containing degenerate codons. The degenerate codons contained the five most preferred mutations that are predicted through B-SIDER scoring and additional amino acids that are included from a degenerate codon. Random mutagenesis through epPCR was applied using GeneMorph II (Agilent) with a mutation rate of 3−4 amino acids per 1 kb, and the constructed library was cloned into pET28a. Ligated vectors were transformed into BL21 (DE3) cells through electroporation and cultured in an SOC medium for 1 h. The cells were further grown in an LB agar plate (SPL Life Sciences) containing kanamycin and IPTG overnight. Approximately 10^4 colonies per round were visually screened under blue light, and the fluorescence of the separated clones was compared. The most promising clones were subjected to a template for the next round of epPCR.

4.4. Structure Determination of the trGFP2.0 in a Complex with an Aβ Motif

To determine the X-ray crystal structure of trGFP2.0 in a complex with an Aβ motif, we genetically fused a target motif (Table S1) using a flexible GS linker containing a TEV protease recognition sequence. The fusion construct was expressed in *E. coli*, followed by purification, and the linker was cleaved through the addition of a TEV protease. The resulting solution was passed through Ni-NTA agarose resin to remove the TEV protease, followed by size exclusion chromatography to further remove the cleaved linker and histidine tag. The purity of the trGFP2.0 in a complex with the target motif was evaluated using SDS/PAGE. The purified trGFP2.0 in a complex with the target motif was concentrated using an Amicon Ultra Centrifugal Filter.

The data were indexed, integrated, and scaled using HKL2000.[53] The structures of the trGFP2.0 were determined through molecular replacement with a search model of GFP (PDB ID:5B61) using Phaser-MR in Phenix software.[54] Refinement was applied using Phenix, and the models were built with Coot.[55] The structure factors of trGFP2.0 were deposited into the PDB database with PDB ID 8I4O. Crystallographic and refinement statistics are shown in Table S5.

4.5. Fluorescence Measurements

The fluorescence of GFP and its derivatives was measured using a TECAN infinite M200 microplate reader. Different concentrations of a target motif or Aβ were mixed with the trGFP2.0 (100 nM) in a black 96-well plate (30496, SPL Life Sciences), and the fluorescence emissions were measured when excited at 390 and 460 nm, respectively. The relative signal by the trGFP2.0 (S) was determined by dividing the fluorescence emissions at 520 nm when excited at 390

https://doi.org/10.1021/jacsau.3c00445
JACS Au 2023, 3, 3055−3065

and 460 nm, respectively, namely, $F_{390/520}/F_{460/520}$, after a 20 min incubation period.

$$S = F_{390/520}/F_{460/520}$$

Integration times for excitation at 390 and 460 nm were fixed at 200 and 20 μs, respectively. Fluorescence signals by trGFP2.0 were normalized by dividing the relative signal from the trGFP2.0 by that from a buffer solution, namely, $S^{A\beta-} = F^{A\beta-}_{390/520}/F^{A\beta-}_{460/520}$.

The normalized signal (NS) was calculated as follows

$$Normalized signal\ (NS) = \frac{S^{A\beta+}}{S^{A\beta-}}$$

For instance, when the Aβ in metal-containing DPBS is evaluated, the fluorescence signal measured by mixing metal-containing DPBS and trGFP2.0 becomes the denominator.

4.6. Determination of Extinction Coefficients and Quantum Yields

The extinction coefficients and quantum yields of GFP variants were determined as described elsewhere.[56] Briefly, based on the molar extinction coefficient of NaOH-denatured GFP (44,000 $M^{-1}cm^{-1}$), molar extinction coefficients of GFP variants were calculated. Because trGFP2.0 has an absorbance maximum at 390 nm, Coumarin 153 dissolved in ethanol was used as a standard for the determination of the quantum yields.

4.7. SPR

The binding kinetics of trGFP2.0 were measured using SPR (Biacore T200, Cytiva). The target Aβ motif was immobilized on a sensor chip through an amine coupling. Ethanolamine was used as a blocking agent, and trGFP2.0 was passed through at various concentrations. The signal responses were then subtracted from those of a negative control. The sensorgrams were fit to a 1:1 Langmuir binding model using the supplied software, and the association and disassociation rates were calculated.

4.8. Monitoring of Aβ Oligomerization

The Aβ peptides were purchased from AnaSpec, and the dried peptide containing HFIP was primarily dissolved in DMSO. The designated concentration of Aβ was diluted in a 50 mM phosphate buffer (pH 7.2) and incubated at 37 °C and 200 rpm. Aβ fibrils and oligomers were obtained sequentially using centrifugation (18,000g, 10 min) for fibrils and two different MWCO filters (Amicon Ultra Centrifugal Filter, Merck) for oligomers (>100 K and >30 K) after incubating Aβ42 at 37 °C. For monomer depletion pattern of Aβ under different conditions, designated concentration of Aβ42 or Aβ40 was incubated at 37 °C and 200 rpm, and the solution was sampled at the designated time. The trGFP2.0 (200 nM) and Aβ peptide solution were mixed at a ratio of 1:1, and the ratio of fluorescence intensity was measured. Fibril seeds of Aβ40 were prepared through the incubation of 50 μM Aβ40 at 37 °C and 200 rpm for 1 week.

4.9. Tracking of Spatial Localization of Aβ in Astrocyte Cells

To obtain a primary rat astrocyte culture, the embryonic cortex was dissected from a pregnant female Sprague−Dawley rat (purchased from Koatech, Korea) and trypsinized to obtain single cells. After filtration through a 70 μm cell strainer (BD Falcon), dissociated cells were maintained in Dulbecco's modified Eagle's medium (DMEM, ATCC) with 10% fetal bovine serum (FBS, Gibco) at 37 °C in a 5% CO_2 incubator for 1 day. To separate the primary astrocytes, a culture flask was gently tapped to detach the oligodendrocytes, microglia, and neurons by tapping, and the floating cells were washed out using DPBS (Gibco). The culture flask with attached astrocytes was filled with fresh DMEM-10% FBS medium and incubated at 37 °C in a 10% CO_2 incubator. The primary astrocytes were passed when the culture reach approximately 70% confluency and used at passage two (P2) for the experiments. These procedures were approved by the Institutional Animal Care and Use Committee (IACUC) at KAIST.

For the confocal imaging experiments, 3×10^3 astrocyte cells per well were plated into a 96-well plate. In addition, Aβ42 (Bachem) dissolved in DMSO was diluted in DPBS and then treated by dropping a 50 μL of Aβ42-DPBS solution onto the cells 2 days after cell plating, followed by the addition of trGFP2.0 into each well after 30 min in the same manner as Aβ42 treatment. Astrocyte cells were fixed for immunostaining or imaged for live imaging 30 min after incubation with the trGFP2.0. The astrocyte membrane was labeled using a PKH26 kit (Sigma-Aldrich) according to the manufacturer's instructions for live cell imaging prior to the treatment of Aβ42 and trGFP2.0. The cells were fixed using 4% paraformaldehyde for 20 min, permeabilized using 0.3% Triton-X100 in DPBS for 15 min, and incubated in a blocking solution (10% FBS, 1% BSA, and 0.1% Tween-20 in DPBS) for 1 h. The blocking solution was replaced with a primary antibody diluted in a blocking solution, after which the solution was rinsed five times with 0.1% Tween-20 in DPBS (PBS-T), followed by incubation with a secondary antibody in the blocking solution again for 1 h. After washing out using PBS-T, the cells were imaged. The antibodies used were anti-Aβ (1:500, Cell Signaling Technology), anti-EGFP (1:2000, Invitrogen), anti-βIII-Tublin (1:2000, Santa Cruz), anti-Rabbit conjugated-Alexa594 (1:1000, Thermo Fisher Scientific), anti-Chicken conjugated-Alexa488 (1:2000, Thermo Fisher Scientific), and anti-Mouse conjugated-Alexa647 (1:2000, Thermo Fisher Scientific). The confocal images were obtained by using a 20x objective lens, and the trGFP2.0 signal was counted through the "object count" function in NIS-element AR imaging software (Nikon) through the DAPI/EGFP ratio view.

For live cell confocal imaging, a Nikon A1R and an AX microscope (Nikon Instrument) with a temperature and CO_2-incubation system (Live Cell Instrument) were used. Detectors of the confocal microscopes were set to acquire ratiometric images at 500−550 nm for 405 nm. To minimize interference with a close wavelength range in the case of a 488 nm laser, the fluorescence detection wavelength at 510−550 nm for 488 nm excitation was adopted. To acquire a wide field of view (FOV), the Large Image Acquisition function was applied, and then the acquired images were stitched together in a 3 × 3 configuration.

■ ASSOCIATED CONTENT

Supporting Information

The Supporting Information is available free of charge at https://pubs.acs.org/doi/10.1021/jacsau.3c00445.

Protein sequences used in this study, introduced mutations during directed evolution, data collection and refinement statistics of crystal structure, trGFP2.0 design procedure, FPLC analysis, general characterization, monitoring Aβ oligomerization, and tracking Aβ localization (PDF)

■ AUTHOR INFORMATION

Corresponding Author

Hak-Sung Kim − *Departement of Biological Sciences, Korea Advanced Institute of Science and Technology (KAIST), Daejeon 34141, Korea;* orcid.org/0000-0002-4034-1892; Email: hskim76@kaist.ac.kr

Authors

Tae-Geun Yu − *Departement of Biological Sciences, Korea Advanced Institute of Science and Technology (KAIST), Daejeon 34141, Korea;* Present Address: Thayer School of Engineering, Dartmouth College, Hanover 03755, New Hampshire, USA

Jinsu Lee − *Departement of Biological Sciences, Korea Advanced Institute of Science and Technology (KAIST), Daejeon 34141, Korea*

https://doi.org/10.1021/jacsau.3c00445
JACS Au 2023, 3, 3055−3065

Jungmin Yoon − *Departement of Biological Sciences, Korea Advanced Institute of Science and Technology (KAIST), Daejeon 34141, Korea*
Jung Min Choi − *School of Food Biotechnology and Nutrition, Kyungsung University, Busan 48434, Korea*
Dong-Gun Kim − *Departement of Biological Sciences, Korea Advanced Institute of Science and Technology (KAIST), Daejeon 34141, Korea;* Present Address: Samsung Bioepis, Incheon 21987, Korea.
Won Do Heo − *Departement of Biological Sciences, Korea Advanced Institute of Science and Technology (KAIST), Daejeon 34141, Korea*
Ji-Joon Song − *Departement of Biological Sciences, Korea Advanced Institute of Science and Technology (KAIST), Daejeon 34141, Korea;* orcid.org/0000-0001-7120-6311

Complete contact information is available at: https://pubs.acs.org/10.1021/jacsau.3c00445

Author Contributions

CRediT: **Tae-Geun Yu** conceptualization, formal analysis, investigation, writing-original draft, writing-review & editing; **Jinsu Lee** formal analysis, investigation, writing-original draft; **Jungmin Yoon** formal analysis, investigation, writing-original draft; **Jung-min Choi** formal analysis, investigation, writing-original draft; **Dong-Gun Kim** formal analysis, investigation; **Won Do Heo** funding acquisition, supervision, writing-review & editing; **Ji-Joon Song** funding acquisition, supervision, writing-review & editing; **Hak-Sung Kim** funding acquisition, supervision, writing-original draft, writing-review & editing.

Notes

The authors declare no competing financial interest.

■ ACKNOWLEDGMENTS

This research was supported by a National Research Foundation of Korea (NRF) grant funded by the Ministry of Science and ICT (NRF-2021R1A2C201421811 to H.-S.K., 2020R1A2C301474213 to W.D.H.) and Basic Science Research Program through the National Research Foundation of Korea (NRF) funded by the Ministry of Education (2019R1I1A1A01040965 to J.S.).

■ REFERENCES

(1) Oates, M. E.; Romero, P.; Ishida, T.; Ghalwash, M.; Mizianty, M. J.; Xue, B.; Dosztanyi, Z.; Uversky, V. N.; Obradovic, Z.; Kurgan, L.; et al. D2P2: database of disordered protein predictions. *Nucleic Acids Res.* **2012**, *41* (D1), D508−D516.
(2) Uversky, V. N. Recent developments in the field of intrinsically disordered proteins: intrinsic disorder−based emergence in cellular biology in light of the physiological and pathological liquid−liquid phase transitions. *Annu. Rev. Biophys.* **2021**, *50* (1), 135−156.
(3) Oldfield, C. J.; Dunker, A. K. Intrinsically disordered proteins and intrinsically disordered protein regions. *Annu. Rev. Biochem.* **2014**, *83* (1), 553−584.
(4) Pedley, A. M.; Boylan, J. P.; Chan, C. Y.; Kennedy, E. L.; Kyoung, M.; Benkovic, S. J. Purine biosynthetic enzymes assemble into liquid-like condensates dependent on the activity of chaperone protein HSP90. *J. Biol. Chem.* **2022**, *298* (5), No. 101845.
(5) Lu, Y.; Sharma, B.; Soon, W. L.; Shi, X.; Zhao, T.; Lim, Y. T.; Sobota, R. M.; Hoon, S.; Pilloni, G.; Usadi, A.; et al. Complete sequences of the velvet worm slime proteins reveal that slime formation is enabled by disulfide bonds and intrinsically disordered regions. *Adv. Sci.* **2022**, *9* (18), No. 2201444.
(6) Chiti, F.; Dobson, C. M. Protein misfolding, amyloid formation, and human disease: a summary of progress over the last decade. *Annu. Rev. Biochem.* **2017**, *86* (1), 27−68.
(7) Iadanza, M. G.; Jackson, M. P.; Hewitt, E. W.; Ranson, N. A.; Radford, S. E. A new era for understanding amyloid structures and disease. *Nat. Rev. Mol. Cell Biol.* **2018**, *19* (12), 755−773.
(8) Liu, L.; Li, Q.; Zhang, S.; Wang, X.; Hoffmann, S. V.; Li, J.; Liu, Z.; Besenbacher, F.; Dong, M. Identification of a Novel Parallel *β*-Strand Conformation within Molecular Monolayer of Amyloid Peptide. *Adv. Sci.* **2016**, *3* (6), No. 1500369.
(9) Wu, K.; Bai, H.; Chang, Y.-T.; Redler, R.; McNally, K. E.; Sheffler, W.; Brunette, T.; Hicks, D. R.; Morgan, T. E.; Stevens, T. J.; et al. De novo design of modular peptide-binding proteins by superhelical matching. *Nature* **2023**, *616* (7957), 581−589.
(10) Jackson, C.; Anderson, A.; Alexandrov, K. The present and the future of protein biosensor engineering. *Curr. Opin. Struct. Biol.* **2022**, *75*, No. 102424.
(11) Rodriguez, E. A.; Campbell, R. E.; Lin, J. Y.; Lin, M. Z.; Miyawaki, A.; Palmer, A. E.; Shu, X.; Zhang, J.; Tsien, R. Y. The growing and glowing toolbox of fluorescent and photoactive proteins. *Trends Biochem. Sci.* **2017**, *42* (2), 111−129.
(12) Quijano-Rubio, A.; Yeh, H.-W.; Park, J.; Lee, H.; Langan, R. A.; Boyken, S. E.; Lajoie, M. J.; Cao, L.; Chow, C. M.; Miranda, M. C.; et al. De novo design of modular and tunable protein biosensors. *Nature* **2021**, *591* (7850), 482−487.
(13) Necci, M.; Piovesan, D.; Tosatto, S. C.; et al. Critical assessment of protein intrinsic disorder prediction. *Nat. Methods* **2021**, *18* (5), 472−481.
(14) Uversky, V. N. Intrinsically disordered proteins and their "mysterious"(meta) physics. *Front. Phys.* **2019**, *7*, 10.
(15) Fernandez-Flores, A. A review of amyloid staining: methods and artifacts. *Biotechnol. Histochem.* **2011**, *86* (5), 293−301.
(16) Schreiber, G.; Keating, A. E. Protein binding specificity versus promiscuity. *Curr. Opin. Struct. Biol.* **2011**, *21* (1), 50−61.
(17) Amaro, M.; Wellbrock, T.; Birch, D. J.; Rolinski, O. J. Inhibition of beta-amyloid aggregation by fluorescent dye labels. *Appl. Phys. Lett.* **2014**, *104* (6), No. 063704.
(18) Wägele, J.; De Sio, S.; Voigt, B.; Balbach, J.; Ott, M. How fluorescent tags modify oligomer size distributions of the Alzheimer peptide. *Biophys. J.* **2019**, *116* (2), 227−238.
(19) Irgen-Gioro, S.; Yoshida, S.; Walling, V.; Chong, S. Fixation can change the appearance of phase separation in living cells. *eLife* **2022**, *11*, No. e79903.
(20) Bishop, D. P.; Cole, N.; Zhang, T.; Doble, P. A.; Hare, D. J. A guide to integrating immunohistochemistry and chemical imaging. *Chem. Soc. Rev.* **2018**, *47* (11), 3770−3787.
(21) Watt, A. D.; Perez, K. A.; Rembach, A.; Sherrat, N. A.; Hung, L. W.; Johanssen, T.; McLean, C. A.; Kok, W. M.; Hutton, C. A.; Fodero-Tavoletti, M.; et al. Oligomers, fact or artefact? SDS-PAGE induces dimerization of *β*-amyloid in human brain samples. *Acta Neuropathol.* **2013**, *125*, 549−564.
(22) Cabantous, S.; Terwilliger, T. C.; Waldo, G. S. Protein tagging and detection with engineered self-assembling fragments of green fluorescent protein. *Nat. Biotechnol.* **2005**, *23* (1), 102−107.
(23) Romei, M. G.; Boxer, S. G. Split green fluorescent proteins: scope, limitations, and outlook. *Annu. Rev. Biophys.* **2019**, *48* (1), 19−44.
(24) Podracky, C. J.; An, C.; DeSousa, A.; Dorr, B. M.; Walsh, D. M.; Liu, D. R. Laboratory evolution of a sortase enzyme that modifies amyloid-*β* protein. *Nat. Chem. Biol.* **2021**, *17* (3), 317−325.
(25) Bracha, D.; Walls, M. T.; Brangwynne, C. P. Probing and engineering liquid-phase organelles. *Nat. Biotechnol.* **2019**, *37* (12), 1435−1445.
(26) Huang, Y.-m.; Banerjee, S.; Crone, D. E.; Schenkelberg, C. D.; Pitman, D. J.; Buck, P. M.; Bystroff, C. Toward computationally designed self-reporting biosensors using leave-one-out green fluorescent protein. *Biochemistry* **2015**, *54* (40), 6263−6273.
(27) Lundqvist, M.; Thalén, N.; Volk, A.-L.; Hansen, H. G.; von Otter, E.; Nygren, P.-Å.; Uhlen, M.; Rockberg, J. Chromophore pre-

maturation for improved speed and sensitivity of split-GFP monitoring of protein secretion. *Sci. Rep.* **2019**, *9* (1), No. 310.
(28) Kent, K. P.; Oltrogge, L. M.; Boxer, S. G. Synthetic control of green fluorescent protein. *J. Am. Chem. Soc.* **2009**, *131* (44), 15988−15989.
(29) Köker, T.; Fernandez, A.; Pinaud, F. Characterization of split fluorescent protein variants and quantitative analyses of their self-assembly process. *Sci. Rep.* **2018**, *8* (1), No. 5344.
(30) Deng, A.; Boxer, S. G. Structural insight into the photochemistry of split green fluorescent proteins: A unique role for a his-tag. *J. Am. Chem. Soc.* **2018**, *140* (1), 375−381.
(31) Kim, B. B.; Wu, H.; Hao, Y. A.; Pan, M.; Chavarha, M.; Zhao, Y.; Westberg, M.; St-Pierre, F.; Wu, J. C.; Lin, M. Z. A red fluorescent protein with improved monomericity enables ratiometric voltage imaging with ASAP3. *Sci. Rep.* **2022**, *12* (1), No. 3678.
(32) Ding, Y.; Li, J.; Enterina, J. R.; Shen, Y.; Zhang, I.; Tewson, P. H.; Mo, G. C.; Zhang, J.; Quinn, A. M.; Hughes, T. E.; et al. Ratiometric biosensors based on dimerization-dependent fluorescent protein exchange. *Nat. Methods* **2015**, *12* (3), 195−198.
(33) Brejc, K.; Sixma, T. K.; Kitts, P. A.; Kain, S. R.; Tsien, R. Y.; Ormö, M.; Remington, S. J. Structural basis for dual excitation and photoisomerization of the Aequorea victoria green fluorescent protein. *Proc. Natl. Acad. Sci. U.S.A.* **1997**, *94* (6), 2306−2311.
(34) Huang, Y.-m.; Bystroff, C. Complementation and reconstitution of fluorescence from circularly permuted and truncated green fluorescent protein. *Biochemistry* **2009**, *48* (5), 929−940.
(35) Nasu, Y.; Shen, Y.; Kramer, L.; Campbell, R. E. Structure-and mechanism-guided design of single fluorescent protein-based biosensors. *Nat. Chem. Biol.* **2021**, *17* (5), 509−518.
(36) Huang, Y. M.; Nayak, S.; Bystroff, C. Quantitative in vivo solubility and reconstitution of truncated circular permutants of green fluorescent protein. *Protein Sci.* **2011**, *20* (11), 1775−1780.
(37) Yu, T.-G.; Kim, H.-S.; Choi, Y. B-SIDER: computational algorithm for the design of complementary β-sheet sequences. *J. Chem. Inf. Model.* **2019**, *59* (10), 4504−4511.
(38) Choi, Y. Computational Identification and Design of Complementary β-Strand Sequences. In *Computational Peptide Science: Methods and Protocols*; Springer, 2022; pp 83−94.
(39) Pédelacq, J.-D.; Cabantous, S.; Tran, T.; Terwilliger, T. C.; Waldo, G. S. Engineering and characterization of a superfolder green fluorescent protein. *Nat. Biotechnol.* **2006**, *24* (1), 79−88.
(40) Oltrogge, L. M.; Wang, Q.; Boxer, S. G. Ground-state proton transfer kinetics in green fluorescent protein. *Biochemistry* **2014**, *53* (37), 5947−5957.
(41) Kaur, J.; Yadav, N. S.; Singh, M. K.; Khan, M. J.; Sen, S.; Dixit, A.; Choudhury, D. Role of Ser65, His148 and Thr203 in the organic solvent-dependent spectral shift in green fluorescent protein. *Photochem. Photobiol.* **2019**, *95* (2), 543−555.
(42) Lee, S.-C.; Park, K.; Han, J.; Lee, J.-j.; Kim, H. J.; Hong, S.; Heu, W.; Kim, Y. J.; Ha, J.-S.; Lee, S.-G.; et al. Design of a binding scaffold based on variable lymphocyte receptors of jawless vertebrates by module engineering. *Proc. Natl. Acad. Sci. U.S.A.* **2012**, *109* (9), 3299−3304.
(43) Linse, S.; Scheidt, T.; Bernfur, K.; Vendruscolo, M.; Dobson, C. M.; Cohen, S. I.; Sileikis, E.; Lundqvist, M.; Qian, F.; O'Malley, T.; et al. Kinetic fingerprints differentiate the mechanisms of action of anti-Aβ antibodies. *Nat. Struct. Mol. Biol.* **2020**, *27* (12), 1125−1133.
(44) Zhang, Y.; Rempel, D. L.; Zhang, J.; Sharma, A. K.; Mirica, L. M.; Gross, M. L. Pulsed hydrogen−deuterium exchange mass spectrometry probes conformational changes in amyloid beta (Aβ) peptide aggregation. *Proc. Natl. Acad. Sci. U.S.A.* **2013**, *110* (36), 14604−14609.
(45) Burra, G.; Maina, M. B.; Serpell, L. C.; Thakur, A. K. Nucleation-dependent aggregation kinetics of Yeast Sup35 fragment GNNQQNY. *J. Mol. Biol.* **2021**, *433* (3), No. 166732.
(46) Prangkio, P.; Yusko, E. C.; Sept, D.; Yang, J.; Mayer, M. Multivariate analyses of amyloid-beta oligomer populations indicate a connection between pore formation and cytotoxicity. *PLoS One* **2012**, *7* (10), No. e47261.
(47) Liu, Y.-H.; Bu, X.-L.; Liang, C.-R.; Wang, Y.-R.; Zhang, T.; Jiao, S.-S.; Zeng, F.; Yao, X.-Q.; Zhou, H.-D.; Deng, J.; Wang, Y. J. An N-terminal antibody promotes the transformation of amyloid fibrils into oligomers and enhances the neurotoxicity of amyloid-beta: the dust-raising effect. *J. Neuroinflammation* **2015**, *12* (1), 1−8.
(48) Lee, M.-C.; Yu, W.-C.; Shih, Y.-H.; Chen, C.-Y.; Guo, Z.-H.; Huang, S.-J.; Chan, J. C.; Chen, Y.-R. Zinc ion rapidly induces toxic, off-pathway amyloid-β oligomers distinct from amyloid-β derived diffusible ligands in Alzheimer's disease. *Sci. Rep.* **2018**, *8* (1), No. 4772.
(49) Weibull, M. G. M.; Simonsen, S.; Oksbjerg, C. R.; Tiwari, M. K.; Hemmingsen, L. Effects of Cu (II) on the aggregation of amyloid-β. *JBIC, J. Biol. Inorg. Chem.* **2019**, *24* (8), 1197−1215.
(50) Faller, P.; Hureau, C.; Berthoumieu, O. Role of metal ions in the self-assembly of the Alzheimer's amyloid-β peptide. *Inorg. Chem.* **2013**, *52* (21), 12193−12206.
(51) Yamamoto, N.; Taniura, H.; Suzuki, K. Insulin inhibits Aβ fibrillogenesis through a decrease of the GM1 ganglioside-rich microdomain in neuronal membranes. *J. Neurochem.* **2010**, *113* (3), 628−636.
(52) Flagmeier, P.; De, S.; Michaels, T. C.; Yang, X.; Dear, A. J.; Emanuelsson, C.; Vendruscolo, M.; Linse, S.; Klenerman, D.; Knowles, T. P.; Dobson, C. M. Direct measurement of lipid membrane disruption connects kinetics and toxicity of Aβ42 aggregation. *Nat. Struct. Mol. Biol.* **2020**, *27* (10), 886−891.
(53) Otwinowski, Z.; Minor, W. Processing of X-ray diffraction data collected in oscillation mode. In *Methods Enzymology*; Elsevier, 1997; Vol. *276*, pp 307−326.
(54) McCoy, A. J.; Grosse-Kunstleve, R. W.; Adams, P. D.; Winn, M. D.; Storoni, L. C.; Read, R. J. Phaser crystallographic software. *J. Appl. Crystallogr.* **2007**, *40* (4), 658−674.
(55) Emsley, P.; Lohkamp, B.; Scott, W.; Cowtan, K. Features and development of Coot. *Acta Crystallogr., Sect. D: Biol. Crystallogr.* **2010**, *66* (Pt 4), 486−504, DOI: 10.1107/S0907444910007493.
(56) Cranfill, P. J.; Sell, B. R.; Baird, M. A.; Allen, J. R.; Lavagnino, Z.; De Gruiter, H. M.; Kremers, G.-J.; Davidson, M. W.; Ustione, A.; Piston, D. W. Quantitative assessment of fluorescent proteins. *Nat. Methods* **2016**, *13* (7), 557−562.

https://doi.org/10.1021/jacsau.3c00445
JACS Au 2023, 3, 3055−3065